Resolving sub-population dynamics in a promiscuous enzyme active site using tethered substrate analogs and 2D IR spectroscopy

Tayler D. Hill†, Hannah H. Lepird†, Sunil Basnet, Joanna A. Hughes, Blaze W. Rightnowar, and Sean D. Moran*

School of Chemical and Biomolecular Sciences, Southern Illinois University Carbondale, 1245 Lincoln Drive MC 4409, Carbondale, IL 62901

Keywords: Enzyme, dynamics, solvation, disorder, 2D IR spectroscopy

ABSTRACT

Protein motion is central to enzymatic catalysis but the influence of ultrafast (femtosecond - picosecond) fluctuations on chemical reaction steps remains poorly understood. One barrier to uniting experiment and theory is difficulty in resolving the dynamics of configurational sub-populations from those of an ensemble. Here we use ultrafast two-dimensional infrared (2D IR) spectroscopy to examine the fluctuations about a vibrationally labeled substrate analog linked to the active site of *Pyrococcus horikoshii* ene-reductase (*Ph*ENR) in two orientations mimicking proposed reactive and inactive reactant states. Frequency fluctuation correlation functions (FFCFs) derived from 2D IR experiments show a near-quantitative tradeoff between fast (<1 ps) and slow (>5 ps) motions upon rotation of the analog as well as enhanced ensemble heterogeneity and a unique ~10 cm^{-1} oscillation in the putative reactive configuration. These observations suggest divergent dynamics among distinct reactant state sub-populations and establish *Ph*ENR as a useful model system for continued studies.

The participation of protein dynamics in enzymatic catalysis is a longstanding question in biophysics with important implications for understanding evolutionary processes and improving approaches to *de novo* enzyme design.[1-5] The fundamental problem is how a barrier-crossing event that takes a few tens of femtoseconds is produced more often (vs. bulk solvent) by longer-timescale stochastic motions of the active site and surrounding scaffold.[6] In general terms, stochastic fluctuations of a pre-organized active site influence the efficiency with which reactive configurations are sampled.[7,8] Combined with electrostatic transition state (TS) stabilization,[9] this can result in substantial lowering of the free energy of activation.[10] Recent work in the field also implicates specific low-frequency (fs-ps) motions along reaction coordinates in rate enhancement.[11] These have been formalized Marcus-like models of activated tunneling in H-atom transfer enzymes[12-14] and protein promoting vibrations that compress reactant state (RS) species toward TS configurations.[6,15] In some cases, a subset of catalytically relevant motions may occur far from a TS.[16] Also, slower conformational motions in an RS can prepare sets of sub-ensembles with individual rate constants that contribute unequally to the overall reactive flux.[17,18] While modern simulations are capable of reconciling these effects, the hierarchical nature of protein dynamics and complex ensemble behaviors make it difficult to obtain direct experimental support for theoretical models.

Among current techniques, ultrafast two-dimensional infrared (2D IR) spectroscopy is particularly well-suited to detect condensed phase dynamics in the fs-ps regime.[19-21] In a 2D IR experiment, a series of mid-IR laser pulses is used to excite (pump) and measure (probe) vibrations of a molecular ensemble after a variable waiting time (T); in macromolecules, unique vibrational labels can be used to obtain site-specific information.[22-25] Environmental fluctuations during T cause a loss of frequency correlation, and time-resolved 2D IR can be used to extract a frequency fluctuation correlation function (FFCF) that quantifies the magnitudes and timescales of dynamical process that contribute to the ensemble lineshape.[26-29] This strategy has been applied to a number of enzymes,[30-34] and although FFCFs can clearly depend on compositions[32-34] and solution conditions,[35] broad IR signals make it difficult to distinguish multi-timescale dynamics of a single configuration from those of discrete slowly-interconverting sub-ensembles.

We selected *Pyrococcus horikoshii* ene-reductase (*Ph*ENR) as a model enzyme to test the configurational dependence of fast RS-like dynamics. *Ph*ENR is a promiscuous enzyme that catalyzes the reduction of activated unsaturated organic compounds via hydride transfer from a flavin mononucleotide (FMN) cofactor and proton transfer from a nearby amino acid side chain or H_2O.[36,37] In a crystal structure reported by Steinkellner *et al*.[37]

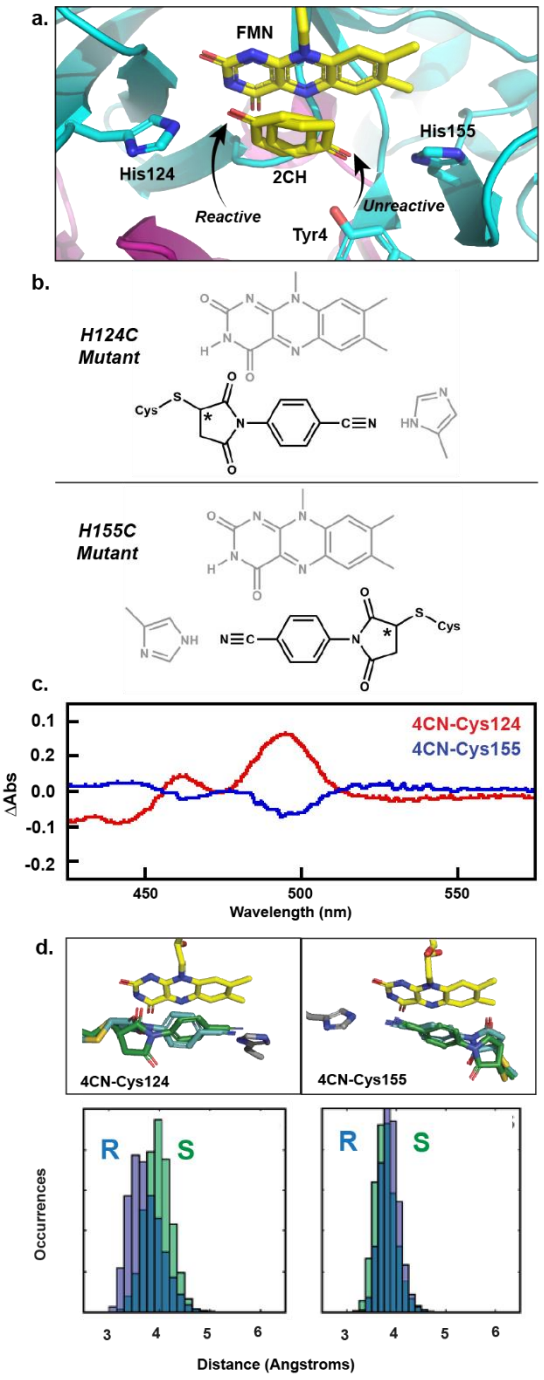

Figure 1. *Ph*ENR model system. a. Detail of the *Ph*ENR active site with two bound orientations of 2CH (PDB ID: 3ZOG). b. Covalently attached aryl-nitrile labels mimicking the 2CH orientations. Stereocenters are indicated with asterisks. c. FMN UV-vis difference spectra (labeled – unlabeled) for 4CN-Cys124 (red) and 4CN-Cys155 (blue). d. *Top:* Representative label conformations for R (cyan) and S (green) label enantiomers. *Bottom:* Histograms showing FMN N5 – label C1 distances over 10 ns MD trajectories.

*Ph*ENR binds the substrate 2-cyclohexenone (2CH) in two nearly isoenergetic configurations separated by a ~180° rotation relative to the FMN (**Figure 1a**). Putative reactive and inactive states were assigned based

equilibrium H^+ donor-acceptor distances between the reactive C=C and Tyr4,[37] but the dynamical natures of the two states were not considered. Here we examine the dynamics of a covalently tethered aryl-nitrile label that mimics the H-bonding and π-electron characteristics of the substrate in each of two configurations (**Figure 1b**).

Reaction of the label precursor 4-cyano-N-phenylmaleimide with His124Cys and His155Cys *Ph*ENR mutants produced a pair of labeled enzymes termed 4CN-Cys124 and 4CN-Cys155 *Ph*ENR, respectively. The labeling reactions proceeded to ~70% completion and shifts in the FMN UV-vis absorbance were observed upon adduct formation (**Figure 1c**). In 4CN-Cys124 *Ph*ENR, a ~4 nm red shift coincides with the perturbation induced by the competitive inhibitor p-hydroxybenzaldehyde (**Figure S1**), but a ~ 2 nm blue shift occurs in 4CN-Cys155 *Ph*ENR, indicating that the 4CN-Cys labels make orientation-specific contacts with the cofactor. To gain insight into the conformations of the labels, we modeled their structures using classical molecular dynamics (MD) simulations performed at 300 K with the NPA algorithm, the AMBER10:EHT force field, and implicit H_2O. Because the ligation reaction generates a stereocenter on the succinimide ring,[38] both the R and S enantiomers of each variant were analyzed. We monitored the FMN(N5)-phenyl(C1) distances over 10 ns trajectories and found close correspondence of the mean configurations with the substrate position and narrow distance distributions for all four systems (**Figure 1d**). The 3.5 – 4.0 Å modes of the distributions are consistent with weak π-π stacking[39] and reflect 2CH equilibrium distances (3.6 Å and 4.3 Å) in the crystal structure.[37] The simulations indicate that linker flexibility allows the cyanophenyl groups of the labels to adopt substrate-like configurations almost independently of stereochemistry.

Despite clear differences in the local environments of the 4CN-Cys124 and 4CN-Cys155 labels and opposing perturbations to the FMN, the Fourier transform infrared (FTIR) spectra in two variants are nearly indistinguishable (**Figure 2a**). In both cases, a single broad C≡N stretch feature with a center frequency (ω_{ctr}) of 2,230 cm^{-1} and a full width at half maximum (FWHM) of ~17 cm^{-1} is observed (**Table 1**). There is no discernable Stark shift (*cf.* **Figure S2**), and neither dynamic asymmetry between the two active sites of the homodimer[40] nor mixtures of stereoisomers are resolved. To characterize the dynamics of each variant, we collected absorptive 2D IR spectra at 12 waiting times between 0.2 – 5.0 ps. Representative spectra are shown in **Figure 2b**, and in each, a pair of peaks corresponds to the v(0-1) and v(1-2) transitions of the C≡N stretch. Vibrational lifetimes (T_1) of ~5 ps for both variants (**Table 1**) were found using slice projection theorem (**Figure S3**).[19] At short *T* (0.2 ps) severe diagonal broadening reflects a high degree of ensemble inhomogeneity. At longer *T* (5.0 ps), the

peaks become more circular as correlation between ω_{pump} and ω_{probe} is lost; this effect appears to be more extensive in 4CN-Cys155 *Ph*ENR.

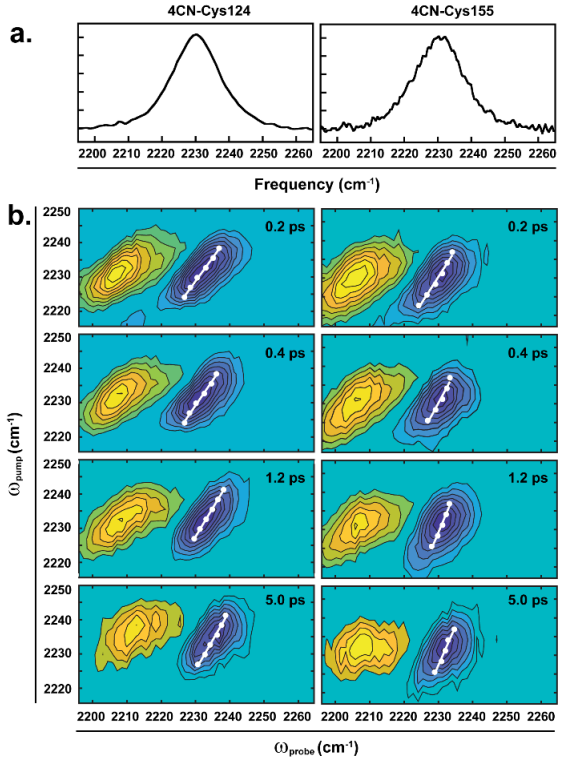

Figure 2. Infrared spectra of 4CN-Cys labeled *Ph*ENR. a. FTIR spectra of 4CN-Cys124 (left) and 4CN-Cys155 (right) *Ph*ENR variants. b. 2D IR spectra of the variants at selected waiting times (see panels) showing v(0-1) (blue) and v(1-2) (yellow) transitions of the CN stretch. The lowest contours about zero are omitted for clarity. Center line points across 0.5 x I_{01} and linear fits are shown in white.

Table 1. FTIR and lifetime parameters for labeled *Ph*ENR variants.

Parameter	4CN-Cys124	4CN-Cys155
ω_{ctr} (cm^{-1})	2230.2 ± 0.1	2230.3 ± 0.1
FWHM (cm^{-1})	17.1 ± 0.1	17.7 ± 0.2
T_1 (ps)	5.1 ± 0.1	5.3 ± 0.3

Standard error reported

The FFCF of the isolated C≡N stretch can be formulated as a sum of terms representing homogeneous and inhomogeneous contributions to the total lineshape.[26-28] Neglecting the small influence of orientational dephasing on macromolecular spectra,[26, 32] the homogeneous linewidth ($\Gamma = 1/\pi T_2$) is given by a homogeneous dephasing time (T_2) that combines effects of pure dephasing (T_2^*) and vibrational relaxation (T_1) via $1/T_2 = 1/T_2^* + 1/2T_1$.[26-

[28,32] Because T_1 was measured independently (**Figure S3**), only T_2^* remains unknown. The time-varying inhomogeneous contributions are given by a sum of Kubo terms, $\sum \Delta\omega_i^2 e^{-t/\tau_i}$, where $\Delta\omega$ and τ are the ranges of frequencies sampled and time constants for each dynamical process, respectively.[41] Combining pure dephasing and inhomogeneous contributions gives the generalized relaxation-free form of the FFCF, *C(t)* (**Equation 1**). Integrating twice gives the lineshape function *g(t)* (**Equation 2**), and the Fourier transform of *g(t)* multiplied by a relaxation factor returns the linear response *I(ω)* (**Equation 3**).[28]

$$C(t) = \frac{2\delta(t)}{T_2^*} + \sum_i \Delta\omega_i^2 e^{t/\tau_i} \quad [1]$$

$$g(t) = \int_0^t \int_0^{\tau'} d\tau' d\tau'' C(\tau'') \quad [2]$$

$$I(\omega) \propto \Re \int_0^\infty e^{i(\omega-\omega_{ctr})t} e^{-g(t)} e^{-t/2T_1} dt \quad [3]$$

A convenient way to extract an FFCF is to measure the evolution of the center line slope (CLS) of a spectral feature over a range of waiting times.[24,26-28,32] Due to low C≡N signals, we employed a slice fitting algorithm that defines center line points above an intensity threshold (see *SI Methods* for details). Representative centerlines using a 50% threshold (0.5 x I_{01}) are overlaid with the spectra in **Figure 2b**. The decay of the CLS (or its reciprocal, by our convention) is proportional to a normalized FFCF that accounts for inhomogeneous dephasing.[26,27,32] First, we analyzed the CLS in 4CN-Cys124 and 4CN-Cys155 *Ph*ENR spectra using the 0.5 x I_{01} threshold, which captures the dynamics within the approximate FWHMs of the v(0-1) features. Mean CLS (0.5 x I_{01}) values from four independent time series are shown in **Figure 3a**. In contrast to the FTIR spectra and measured T_1 values, there is a clear difference between the magnitudes of fast (<1 ps) components and static (>5 ps) offsets between the two variants. The offsets suggest that although the cyanophenyl moieties of the labels are partially solvent exposed, constraints imposed by the active site environment maintain frequency correlations past 5 ps.[28] A phenomenological fit to the data (**Equation 4**) yielded the time constant of the fast decay (τ_1). The amplitudes A_i and the FTIR FWHMs were used to estimate $\Delta\omega_i$ via **Equation 5**.[26]

$$CLS(T) = A_0 + A_1 e^{-T/\tau_1} \quad [4]$$

$$\Delta\omega_i = \sqrt{\frac{A_i}{\sum_i A_i}} \frac{FWHM}{2\sqrt{2\ln(2)}} \quad [5]$$

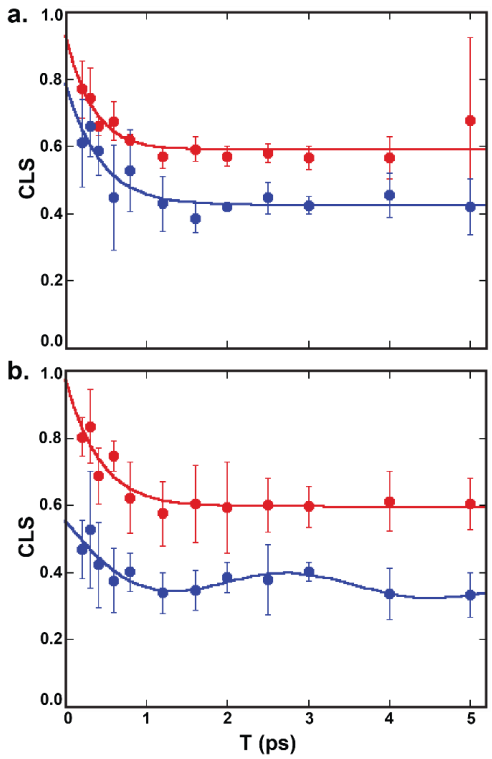

Figure 4. CLS analysis of 4CN-Cys *Ph*ENR variants. a. CLS decays for 4CN-Cys124 (red) and 4CN-Cys155 (blue) labeled *Ph*ENR variants using an intensity threshold of 0.5 x I_{01}. b. CLS decays for 4CN-Cys124 (red) and 4CN-Cys155 (blue) labeled *Ph*ENR variants using an intensity threshold of 0.8 x I_{01}. Solid lines indicate fits to the data using either **Equation 4** or **Equation 6** as described in the text and error bars indicate standard deviations of four independent trials.

To obtain realistic values for T_2^* (and thus T_2 and Γ), we scaled the measured CLS values to fit simulated linear responses (**Equations 1 – 3**) to the experimental FTIR spectra (**Figure S4**).[26,28,29] Values of the FFCF parameters are reported in **Table 2**. Because $\tau_1 \approx 0.4\,ps$ and $\Delta\omega_1 \approx 0.7 - 1.0\,rad\,ps^{-1}$, the fast decays contribute to T_2^* and account for ~50% of the pure dephasing linewidths (Γ^*).[19,30] The associated contributions to total Gaussian (inhomogeneous) width, W_G are relatively minor. The treatment of the fast decay is detailed in the *SI Methods*.

Table 2. FFCF parameters for labeled *Ph*ENR variants.

	CLS with 0.5 x I_{01} threshold		*CLS with 0.8 x I_{01} threshold*	
Parameter	**4CN-Cys124**	**4CN-Cys155**	**4CN-Cys124**	**4CN-Cys155**
$\Delta\omega_0$ (cm^{-1})	6.1 ± 0.1	5.5 ± 0.2	6.2 ± 0.1	5.8 ± 0.2
$\Delta\omega_1$ (cm^{-1})	3.9 ± 0.1	5.1 ± 0.2	3.7 ± 0.2	4.1 ± 0.3
τ_1 (ps)	0.4 ± 0.1	0.4 ± 0.2	0.6 ± 0.2	0.9 ± 0.2
$\Delta\omega_2$ (cm^{-1})	--	--	--	2.5 ± 0.3
τ_2 (ps)	--	--	--	5.7 ± 4.9
T_{osc} (ps)	--	--	--	3.5 ± 0.4
ϕ_{osc} (rad)	--	--	--	1.2 ± 0.3
T_2* (ps)	2.4 ± 0.2	1.4 ± 0.2	2.6 ± 0.2	1.6 ± 0.2
Γ* (cm^{-1})	4.4 ± 0.3	7.3 ± 0.8	4.0 ± 0.4	6.8 ± 0.8
T_2 (ps)	2.0 ± 0.1	1.3 ± 0.1	2.1 ± 0.1	1.4 ± 0.1
Γ (cm^{-1})	5.4 ± 0.3	8.3 ± 0.8	5.1 ± 0.4	7.8 ± 0.8
W_G (cm^{-1})	14.4 ± 0.2	13.1 ± 0.5	14.7 ± 0.3	14.0 ± 0.5

Standard error reported

The picture that emerges is a near quantitative tradeoff between sub-picosecond fluctuations and static frequency distributions upon rotation of the substrate analog in the active site. However, the breadths of the distributions suggest the possibility of multiple slowly converting sub-ensembles that are not distinguished using a broad CLS threshold.[42] Since the frequency resolution of our spectrometer is not sufficient to perform piecewise analysis of the 2D IR spectra, we tested for frequency dependence of the FFCFs by applying a narrower intensity threshold (0.8 x I_{01}) that constrains center line points to within a few cm^{-1} of ω_{ctr}. The CLS decays are shown in **Figure 3b**. For the 4CN-Cys124 variant, the narrow threshold CLS decay mirrors that of obtained with the broader threshold (**Figure 3a**), and **Equations 1 – 5** returned quantitatively identical FFCF parameters (**Table 2**). Thus, the dynamics of the predominant 4CN-Cys124 configuration are indistinguishable from the broader ensemble, and the energy landscape appears uniformly rough. In contrast, the CLS values of the 4CN-Cys155 variant differ with respect to the applied threshold; near ω_{ctr}, the initial value is suppressed and there is evidence for periodic modulation that extends past 5 ps. We added an exponentially damped cosine term to the trial function (**Equation 6**) and applied the same analysis to fit the linear response (**Figure S4**).[33]

$$CLS(T) = A_0 + A_1 e^{-T/\tau_1} + A_2 e^{-T/\tau_2} \cos\left(\frac{2\pi T}{T_{osc}} + \phi_{osc}\right) \qquad [6]$$

The resulting FFCF parameters (**Table 2**) show that the tradeoff between fast and static contributions is maintained, but the 3.5 ps (~10 cm^{-1}) oscillatory component “borrows” amplitude from the exponential decay.

Clearly, the dynamics of the predominant 4CN-Cys155 configuration are distinct from the edges of its ensemble and differ qualitatively from the 4CN-Cys124 variant. This variation may be a result of a more complex energy landscape, a mixture of two stereoisomers, or both.

Similar underdamped CLS oscillations have been observed in the TS analog of FDH and were convincingly attributed to low-frequency gating motions of the surrounding scaffold.[33,34] Superficially, it seems that the same phenomenon may occur uniquely in the 4CN-Cys155 *Ph*ENR mimic of the putative reactive state.[37] Whether any of the observed dynamics are relevant to catalysis remains unknown, and it is notable that 2CH reduction by the related enzyme *P. putida* morphinone reductase showed no evidence of gated tunneling.[43] Furthermore, it is surprising to observe any underdamped behavior in a measurement of an incoherently fluctuating ensemble of ~10^{12} protein molecules, so we must consider the possibility that the lineshape oscillation is laser-induced. The pump and probe pulses overlap with a weak bend-libration mode of the solvent (H_2O) that relaxes within ~200 fs and may excite low-lying modes of the protein.[44] Nevertheless, dynamics induced by weak perturbations are likely to occur in native modes of the system.[45] We hypothesize that the less-constrained 4CN-Cys155 *Ph*ENR environment is more susceptible to such effects.

In summary, we have shown that sufficient separation of RS-like complexes of *Ph*ENR containing a substrate analog allow distinct dynamical signatures to be recovered with 2D IR spectroscopy. Orientation-dependent variations include divergences between sub-picosecond and long-lived fluctuations, as well as an underdamped oscillation that we tentatively attribute to laser induced excitation of low-frequency protein modes. Currently, this information is confined to regions occupied by the activating C=O (C≡N) moiety of the substrate (label). In future studies, we will aim to characterize dynamics in the region of the reactive C=C bond and correlations between active site and scaffold dynamics. Fermi resonant aryl-azide analogs[46-48] and genetically encoded non-natural amino acid labels[25,41] may be well-suited for these purposes. A comprehensive description will require analogous experiments in the reduced (H^- donating) state of the FMN. Furthermore, determining whether any motions detected by 2D IR are relevant to catalysis will likely require high-resolution structures, detailed simulations, mutagenic studies, and activity assays. However, we expect our study to motivate renewed consideration of sub-ensemble dynamics in enzyme-substrate reactant ground states. We plan to continue using *Ph*ENR as a model enzyme because – perhaps counterintuitively – divergent dynamics within its disordered RS may provide a critical test of the importance of motions in catalysis.

EXPERIMENTAL METHODS.

The *Ph*ENR variants were expressed in *E. coli*, purified using metal affinity chromatography, and reacted with 4-cyano-N-phenylmaleimide at room temperature in pH 7.5 sodium phosphate buffer. Unreacted labels were removed by size-exclusion chromatography and the labeled enzymes were concentrated to ~5 - 6 mM using ultrafiltration. MD simulations based on the crystal structure of the 2CH complex (PDB ID: 3ZOG[37]) were performed in MOE (CCG Inc., Montreal, Quebec). UV-vis, FTIR, and 2D IR spectra were collected at ambient conditions. For 2D IR, ~25 μJ, 100 fs pulses centered at 4500 nm were directed into a PhaseTech Spectroscopy (Madison, WI) 2DQuick Array pulse shaping spectrometer. Pump and probe beams were spatiotemporally overlapped on samples placed between two 2 mm CaF_2 windows in a demountable liquid cell. All data were processed in MATLAB (MathWorks, Natick, MA). Detailed descriptions of sample preparation, the instrumental setup, and data analysis procedures are provided in the *SI Methods*.

Associated Content.

Supporting information. Detailed description of experimental methods and data processing. Inhibitor binding analysis using UV-vis spectroscopy. FTIR and 2D IR spectra of the free 4CN-M label. C≡N vibrational lifetimes of *Ph*ENR varaints. Simulated linear responses from FFCF parameters.

Author Information.

Corresponding author.

* E-mail: smoran@chem.siu.edu

Author contributions.

† These authors contributed equally to this manuscript.

Acknowledgements.

Research reported in this manuscript was supported by the National Institute of General Medical Sciences (NIGMS) of the National Institutes of Health under award number R35GM119818 (to S.D.M.). This material is based on work supported by the National Science Foundation under award DGE-1545870 (to T.D.H.)

REFERENCES.

1. Agarwal, P. K., A Biophysical Perspective on Enzyme Catalysis. *Biochemistry* **2019,** *58* (6), 438-449.

2. Kamerlin, S. C. L.; Warshel, A., At the dawn of the 21st century: Is dynamics the missing link for understanding enzyme catalysis? *Proteins* **2010,** *78* (6), 1339-1375.

3. Olsson, M. H. M.; Parson, W. W.; Warshel, A., Dynamical Contributions to Enzyme Catalysis: Critical Tests of A Popular Hypothesis. *Chem. Rev.* **2006,** *106* (5), 1737-1756.

4. Warshel, A.; Bora, R. P., Perspective: Defining and quantifying the role of dynamics in enzyme catalysis. *J. Chem. Phys.* **2016,** *144* (18), 180901.

5. Tuñón, I.; Laage, D.; Hynes, J. T., Are there dynamical effects in enzyme catalysis? Some thoughts concerning the enzymatic chemical step. *Arch. Biochem. Biophys.* **2015,** *582*, 42-55.

6. Schramm, V. L.; Schwartz, S. D., Promoting Vibrations and the Function of Enzymes. Emerging Theoretical and Experimental Convergence. *Biochemistry* **2018,** *57* (24), 3299-3308.

7. Jindal, G.; Warshel, A., Misunderstanding the preorganization concept can lead to confusions about the origin of enzyme catalysis. *Proteins* **2017,** *85* (12), 2157-2161.

8. Hammes-Schiffer, S., Catalytic Efficiency of Enzymes: A Theoretical Analysis. *Biochemistry* **2013,** *52* (12), 2012-2020.

9. Warshel, A.; Sharma, P. K.; Kato, M.; Xiang, Y.; Liu, H.; Olsson, M. H. M., Electrostatic Basis for Enzyme Catalysis. *Chem. Rev.* **2006,** *106* (8), 3210-3235.

10. Garcia-Viloca, M.; Gao, J.; Karplus, M.; Truhlar, D. G., How Enzymes Work: Analysis by Modern Rate Theory and Computer Simulations. *Science* **2004,** *303* (5655), 186-195.

11. Hay, S.; Scrutton, N. S., Good vibrations in enzyme-catalysed reactions. *Nat. Chem.* **2012,** *4* (3), 161-168.

12. Nagel, Z. D.; Klinman, J. P., A 21st century revisionist's view at a turning point in enzymology. *Nat. Chem. Biol.* **2009,** *5* (8), 543-550.

13. Cheatum, C. M., Low-Frequency Protein Motions Coupled to Catalytic Sites. *Annu. Rev. Phys. Chem.* **2020,** *71* (1), 267-288.

14. Kohen, A., Role of Dynamics in Enzyme Catalysis: Substantial versus Semantic Controversies. *Acc. Chem. Res.* **2015,** *48* (2), 466-473.

15. Chalopin, Y., The physical origin of rate promoting vibrations in enzymes revealed by structural rigidity. *Sci. Rep.* **2020,** *10* (1), 17465.

16. Antoniou, D.; Schwartz, S. D., Role of Protein Motions in Catalysis by Formate Dehydrogenase. *J. Phys. Chem. B* **2020,** *124* (43), 9483-9489.

17. Callender, R.; Dyer, R. B., The Dynamical Nature of Enzymatic Catalysis. *Acc. Chem. Res.* **2015,** *48* (2), 407-413.

18. Glowacki, D. R.; Harvey, J. N.; Mulholland, A. J., Taking Ockham's razor to enzyme dynamics and catalysis. *Nat. Chem.* **2012,** *4* (3), 169-176.

19. Hamm, P.; Zanni, M., *Concepts and Methods of 2D Infrared Spectroscopy*. Cambridge University Press: Cambridge, 2011.

20. Le Sueur, A. L.; Horness, R. E.; Thielges, M. C., Applications of two-dimensional infrared spectroscopy. *Analyst* **2015,** *140* (13), 4336-4349.

21. Hunt, N. T., 2D-IR spectroscopy: ultrafast insights into biomolecule structure and function. *Chem. Soc. Rev.* **2009,** *38* (7), 1837-1848.

22. Kim, H.; Cho, M., Infrared Probes for Studying the Structure and Dynamics of Biomolecules. *Chem. Rev.* **2013,** *113* (8), 5817-5847.

23. Ghosh, A.; Ostrander, J. S.; Zanni, M. T., Watching Proteins Wiggle: Mapping Structures with Two-Dimensional Infrared Spectroscopy. *Chem. Rev.* **2017,** *117* (16), 10726-10759.

24. Thielges, M. C.; Fayer, M. D., Protein Dynamics Studied with Ultrafast Two-Dimensional Infrared Vibrational Echo Spectroscopy. *Acc. Chem. Res.* **2012,** *45* (11), 1866-1874.

25. Ramos, S.; Horness, R. E.; Collins, J. A.; Haak, D.; Thielges, M. C., Site-specific 2D IR spectroscopy: a general approach for the characterization of protein dynamics with high spatial and temporal resolution. *Phys. Chem. Chem. Phys.* **2019,** *21* (2), 780-788.

26. Kwak, K.; Park, S.; Finkelstein, I. J.; Fayer, M. D., Frequency-frequency correlation functions and apodization in two-dimensional infrared vibrational echo spectroscopy: A new approach. *J. Chem. Phys.* **2007,** *127* (12), 124503.

27. Guo, Q.; Pagano, P.; Li, Y.-L.; Kohen, A.; Cheatum, C. M., Line shape analysis of two-dimensional infrared spectra. *J. Chem. Phys.* **2015,** *142* (21), 212427.

28. Ma, J.; Pazos, I. M.; Gai, F., Microscopic insights into the protein-stabilizing effect of trimethylamine N-oxide (TMAO). *Proc. Natl. Acad. Sci. U.S.A.* **2014,** *111* (23), 8476-8481.

29. Bandaria Jigar, N.; Dutta, S.; Nydegger Michael, W.; Rock, W.; Kohen, A.; Cheatum Christopher, M., Characterizing the dynamics of functionally relevant complexes of formate dehydrogenase. *Proc. Natl. Acad. Sci. U.S.A.* **2010,** *107* (42), 17974-17979.

30. Finkelstein, I. J.; Ishikawa, H.; Kim, S.; Massari, A. M.; Fayer, M. D., Substrate binding and protein conformational dynamics measured by 2D-IR vibrational echo spectroscopy. *Proc. Natl. Acad. Sci. U.S.A.* **2007,** *104* (8), 2637-2642.

31. Kuroda, D. G.; Bauman, J. D.; Challa, J. R.; Patel, D.; Troxler, T.; Das, K.; Arnold, E.; Hochstrasser, R. M., Snapshot of the equilibrium dynamics of a drug bound to HIV-1 reverse transcriptase. *Nat. Chem.* **2013,** *5* (3), 174-181.

32. Thielges, M. C.; Chung, J. K.; Fayer, M. D., Protein Dynamics in Cytochrome P450 Molecular Recognition and Substrate Specificity Using 2D IR Vibrational Echo Spectroscopy. *J. Am. Chem. Soc.* **2011,** *133* (11), 3995-4004.

33. Pagano, P.; Guo, Q.; Kohen, A.; Cheatum, C. M., Oscillatory Enzyme Dynamics Revealed by Two-Dimensional Infrared Spectroscopy. *J. Phys. Chem. Lett.* **2016,** *7* (13), 2507-2511.

34. Pagano, P.; Guo, Q.; Ranasinghe, C.; Schroeder, E.; Robben, K.; Häse, F.; Ye, H.; Wickersham, K.; Aspuru-Guzik, A.; Major, D. T.; Gakhar, L.; Kohen, A.; Cheatum, C. M., Oscillatory Active-Site Motions Correlate with Kinetic Isotope Effects in Formate Dehydrogenase. *ACS Catal.* **2019,** *9* (12), 11199-11206.

35. Cheng, M.; Brookes, J. F.; Montfort, W. R.; Khalil, M., pH-Dependent Picosecond Structural Dynamics in the Distal Pocket of Nitrophorin 4 Investigated by 2D IR Spectroscopy. *J. Phys. Chem. B* **2013,** *117* (49), 15804-15811.

36. Toogood, H. S.; Scrutton, N. S., Discovery, Characterization, Engineering, and Applications of Ene-Reductases for Industrial Biocatalysis. *ACS Catal.* **2018,** *8* (4), 3532-3549.

37. Steinkellner, G.; Gruber, C. C.; Pavkov-Keller, T.; Binter, A.; Steiner, K.; Winkler, C.; Łyskowski, A.; Schwamberger, O.; Oberer, M.; Schwab, H.; Faber, K.; Macheroux, P.; Gruber, K., Identification of promiscuous ene-reductase activity by mining structural databases using active site constellations. *Nat. Commun.* **2014,** *5* (1), 4150.

38. Kim, Y.; Ho, S. O.; Gassman, N. R.; Korlann, Y.; Landorf, E. V.; Collart, F. R.; Weiss, S., Efficient Site-Specific Labeling of Proteins via Cysteines. *Bioconjugate Chem.* **2008,** *19* (3), 786-791.

39. McGaughey, G. B.; Gagné, M.; Rappé, A. K., π-Stacking Interactions: Alive And Well In Proteins. *J. Biol. Chem.* **1998,** *273* (25), 15458-15463.

40. Londergan, C. H.; Baskin, R.; Bischak, C. G.; Hoffman, K. W.; Snead, D. M.; Reynoso, C., Dynamic Asymmetry and the Role of the Conserved Active-Site Thiol in Rabbit Muscle Creatine Kinase. *Biochemistry* **2015,** *54* (1), 83-95.

41. Thielges, M. C.; Axup, J. Y.; Wong, D.; Lee, H. S.; Chung, J. K.; Schultz, P. G.; Fayer, M. D., Two-Dimensional IR Spectroscopy of Protein Dynamics Using Two Vibrational Labels: A Site-Specific Genetically Encoded Unnatural Amino Acid and an Active Site Ligand. *J. Phys. Chem. B* **2011,** *115* (38), 11294-11304.

42. Fenn, E. E.; Fayer, M. D., Extracting 2D IR frequency-frequency correlation functions from two component systems. *J. Chem. Phys.* **2011,** *135* (7), 074502.

43. Basran, J.; Harris, R. J.; Sutcliffe, M. J.; Scrutton, N. S., H-tunneling in the Multiple H-transfers of the Catalytic Cycle of Morphinone Reductase and in the Reductive Half-reaction of the Homologous Pentaerythritol Tetranitrate Reductase. *J. Biol. Chem.* **2003,** *278* (45), 43973-43982.

44. Verma, P. K.; Kundu, A.; Puretz, M. S.; Dhoonmoon, C.; Chegwidden, O. S.; Londergan, C. H.; Cho, M., The Bend+Libration Combination Band Is an Intrinsic, Collective, and Strongly Solute-Dependent Reporter on the Hydrogen Bonding Network of Liquid Water. *J. Phys. Chem. B* **2018,** *122* (9), 2587-2599.

45. Stratt, R. M.; Maroncelli, M., Nonreactive Dynamics in Solution: The Emerging Molecular View of Solvation Dynamics and Vibrational Relaxation. *J. Phys. Chem.* **1996,** *100* (31), 12981-12996.

46. Park, J. Y.; Mondal, S.; Kwon, H.-J.; Sahu, P. K.; Han, H.; Kwak, K.; Cho, M., Effect of isotope substitution on the Fermi resonance and vibrational lifetime of unnatural amino acids modified with IR probe: A 2D-IR and pump-probe study of 4-azido-L-phenyl alanine. *J. Chem. Phys.* **2020,** *153* (16), 164309.

47. Lipkin, J. S.; Song, R.; Fenlon, E. E.; Brewer, S. H., Modulating Accidental Fermi Resonance: What a Difference a Neutron Makes. *J. Phys. Chem. Lett.* **2011,** *2* (14), 1672-1676.

48. Perera, S.; Aikawa, T.; Shaner, S.; Moran, S.; Wang, L., Effects of Intramolecular Group and Solvent on Vibrational Coupling Modes and Strengths of Fermi Resonances in Aryl Azides: A DFT Study of 4-Azidotolune and 4-Azido-N-Phenylmaleimide. *chemRxiv* [Preprint] Oct. 6, **2022** [Version 1]. DOI: 10.26434/chemrxiv-2022-gd3mk